Journal of Biomolecular NMR, **11:** 17–29, 1998.
KLUWER/ESCOM

A NOESY-HSQC simulation program, SPIRIT

Leiming Zhu[a,b], H. Jane Dyson[a] & Peter E. Wright[a,b,*]
[a]*Department of Molecular Biology and* [b]*Skaggs Institute for Chemical Biology, The Scripps Research Institute, La Jolla, CA 92037, USA*

Received 23 June 1997; Accepted 12 August 1997

Key words: isotope-editing efficiency, NMR structural refinement, NOESY-HSQC, spectral simulation, thioredoxin

Abstract

A program SPIRIT (*S*imulation *P*rogram considering *I*ncomplete *R*ecovery of z magnetization and *I*NEPT *T*ransfer efficiency) has been developed to simulate three-dimensional NOESY-HSQC spectra. This program takes into account (1) different transfer efficiency during INEPT and reverse INEPT durations due to differential relaxation rates and ^1J coupling constants; (2) the different effect of the sensitivity-enhancement scheme on CH, CH_2 and CH_3 systems; and (3) incomplete recovery of longitudinal magnetization between scans. The simulation program incorporates anisotropic tumbling mode for symmetric tops, and allows for differential external relaxation rates for protons. Some well-defined internal motions, such as the fast rotation of methyl groups, are taken into account. The simulation program also allows for input of multiple conformations and their relative populations to calculate the average relaxation matrix to account for slow internal motions. With the SPIRIT program, the sensitivity-enhanced NOESY-HSQC experiment can be used directly in the evaluation of the accuracy of structures, which can potentially be improved by direct refinement against the primary data.

Abbreviations: NOESY, nuclear Overhauser enhancement spectroscopy; HSQC, heteronuclear single quantum correlation; INEPT, insensitive nuclei enhanced by polarization transfer.

Introduction

The introduction of 3D and 4D NMR combined with ^{13}C and/or ^{15}N labeling techniques has greatly facilitated spectral assignments and significantly enhanced the ability of NMR in determining biomolecular structures (Bax, 1994). Triple resonance techniques (Ikura et al., 1990; Kay et al., 1990; Cavanagh et al., 1996) make it possible to assign backbone resonances in a conformation-independent manner for proteins as large as ~30 kDa. More resolved NOE peaks, and therefore more distance restraints, can be obtained from ^{13}C and ^{15}N-edited 3D NOESY-HSQC experiments by dispersing the NOE cross peaks in three (or even four) dimensions (Zuiderweg and Fesik, 1989).

However, due to the effects of spin diffusion (Noggle and Schirmer, 1971) and differential INEPT transfer efficiencies, proton-proton distances, the primary input data for solution structure calculations, cannot be accurately estimated from cross-peak intensities in 3D or 4D isotope-edited NOESY spectra. A general approach is to employ very short mixing times (to minimize the spin diffusion effect) and use rather wide distance bounds in structure calculation. However, the use of shorter mixing times leads to fewer and weaker cross peaks and consequently fewer distance constraints. Lower numbers of constraints and loose distance bounds result in less defined structures. These structures are obviously still useful. However, our experience indicates that higher resolution is required to determine the details of the intermolecular interactions, such as in ligand–protein complexes, protein–protein complexes and protein–nucleic acid complexes; these interactions are extremely important both in understanding fundamental biological processes and in drug design.

*To whom correspondence should be addressed.

To take into account the effect of spin diffusion on NOE intensities, it has been common practice to use NOESY simulation in structure determination based mainly on proton homonuclear NMR data (Boelens et al., 1989; Nerdal et al., 1989; Borgias and James, 1990; Post et al., 1990; Zhu and Reid, 1995; Görler and Kalbitzer, 1997). However, 3D NOESY-HSQC simulations have not been introduced into the structure refinement of proteins, RNA, or DNA, all of which can be uniformly ^{13}C and/or ^{15}N-labeled (Clore and Gronenborn, 1989; Nikonowicz et al., 1992; Zimmer and Crothers, 1995). As discussed in detail below, simulation of NOESY-HSQC experiments is even more important than for homonuclear NOESY spectra because, in addition to the spin diffusion effect, the intensity of a cross peak is further affected by one-bond coherence transfer efficiencies (editing efficiencies), which can differ significantly for different spins, especially in sensitivity-enhanced experiments.

We describe a 3D NOESY-HSQC simulation program, SPIRIT (*S*imulation *P*rogram considering *I*ncomplete *R*ecovery of z magnetization and *I*NEPT *T*ransfer efficiency). The major factors affecting the cross-peak intensities are discussed and are incorporated into the simulation program. The simulation program is demonstrated by application to the oxidized *E. coli* thioredoxin system, for which a complete set of resonance assignments (Dyson et al., 1989; Chandrasekhar et al., 1991, 1994) and a high-resolution solution structure (Jeng et al., 1994) have been published, and which can in addition be compared to high-resolution X-ray crystal structures (Katti et al., 1990).

General considerations

In the NMR-based structure determination, the relationship between a NOESY cross-peak intensity and the estimated distance of the corresponding proton pair is assumed to be

$$I_{ij} \propto r_{ij}^{-6} \tag{1}$$

The major factor causing deviation from the above equation is the spin diffusion effect (Noggle and Schirmer, 1971). To alleviate this effect, spectra are either recorded using very short mixing times, or a full Solomon relaxation matrix simulation is employed to account for spin diffusion (Boelens et al., 1989; Nerdal et al., 1989; Borgias and James, 1990; Post et al., 1990; Zhu and Reid, 1995; Görler and Kalbitzer, 1997). When the relaxation delay is not long enough compared to the proton T_1, the NOE intensity is also affected by the extent of M_z recovery between scans (Köck and Griesinger, 1994; Zhu and Reid, 1995; Liu et al., 1996). A 2D NOESY cross-peak intensity can be calculated as (Macura and Ernst, 1980)

$$I_{ij} = M_z^j(0)[\exp(-\mathbf{R}t_m)]_{ij}, \tag{2}$$

where I_{ij} is the cross-peak intensity at ω_i in D1 and ω_j in D2, representing the z-magnetization transfer from I_z^j to I_z^i; $\mathbf{R}$ is the Solomon relaxation matrix; t_m is the mixing time; $M_z^j(0)$ is the longitudinal magnetization immediately before the first pulse of the NOESY pulse sequence,

$$M_z^j(0) = 1 - \sum_{i=1}^{n}[\exp(-\mathbf{R}t_d)]_{ji}, \tag{3}$$

or, if the longitudinal relaxation rates are available, $M_z^j(0)$ can be approximated as

$$M_z^j(0) \approx 1 - \exp(-R_1^j t_d), \tag{4}$$

where t_d is the total M_z recovery time, i.e., the acquisition time plus the relaxation delay.

In a NOESY-HSQC experiment, in addition to the effects discussed above, the INEPT and reverse INEPT transfer efficiencies have to be considered. During the INEPT and reverse INEPT processes, coherence transfer (between I_x^i and $2I_y^iS_z^i$) and relaxation occur simultaneously. If the dipolar interaction is the dominating relaxation mechanism, and denoting the relaxation rate for I_x^i as $R_2^{I_i}$, it can be shown that (Zhu, 1996) the relaxation rate for $2I_y^iS_z^i$ is

$$\begin{aligned} R(2I_y^iS_z^i) &= R_2^{I_i} + R_{1*}^{S_i} - \frac{3\gamma_I^2\gamma_S^2\hbar^2}{10}J^{S_iI_i}(\Omega_S) \\ &= R_2^{I_i} + R_{1**}^{S_i}, \end{aligned} \tag{5}$$

where $R_{1*}^{S_i}$ is part of the (selective) longitudinal relaxation rate of spin S_i, in which the contribution of the dipolar interaction from spin I_i is excluded (for details, see Table 3 of Zhu (1996) for the three-spin case, and Chapter 5 of Cavanagh et al. (1996) for the two-spin case). From Equation (5), it can be seen that $R_{1**}^{S_i} < R_{1*}^{S_i} < R_1^{S_i}$ (where $R_1^{S_i}$ is the (selective) longitudinal relaxation rate for spin S_i); the value of $R_{1**}^{S_i}$ can even be negative, such as in the case of a

nearly isolated $I^i S^i$ two-spin system. Ω_S is the Larmor frequency for spin S_i and $J^{S_i I_i}(\Omega_S)$ is the spectral density for the dipolar interaction between spins I_i and S_i and will be described in more detail later (Equations (14), (16) or (17)). Using the average relaxation rate for I_x^i and $2I_y^i S_z^i$, $R_2^{I_i} + \frac{1}{2}R_{1**}^{S_i}$, as an approximate relaxation rate during the INEPT and reverse INEPT processes, and letting $\mathcal{F}_i^1$ and $\mathcal{F}_i^2$ represent the transfer efficiency for the INEPT process of duration τ_1 and that for the reverse INEPT process of duration τ_2, respectively, one obtains

$$\mathcal{F}_i^1 = \sin(\pi J_i \tau_1) \exp[-(R_2^{I_i} + \tfrac{1}{2}R_{1**}^{S_i})\tau_1] \quad (6)$$

$$\mathcal{F}_i^2 = \sin(\pi J_i \tau_2) \exp[-(R_2^{I_i} + \tfrac{1}{2}R_{1**}^{S_i})\tau_2], \quad (7)$$

where J_i is the one-bond J-coupling constant between S_i and I_i. Since, in biomolecular spin systems, the value of $|R_{1**}^{S_i}|$ is usually much smaller than that of $R_2^{I_i}$, the approximation made in Equations (6) and (7) does not introduce significant errors. Theoretically, the Hamiltonian superoperator and relaxation superoperator do not commute and a rigorous treatment is rather complicated.

In a sensitivity-enhanced experiment, an additional refocusing period (τ_3) is introduced to recover multiple quantum (MQ) coherences, resulting in phase-modulated signals and a $\sqrt{2}$ fold increase in sensitivity (Cavanagh et al., 1991; Palmer et al., 1991). However, the two perpendicular pathways do not have the same amplitude due to different relaxation rates between the two pathways, which is further worsened in the case of $I_n S$ ($n > 1$) moieties, since the extended reverse INEPT transfer efficiencies for the z-magnetization pathway and MQ coherence pathway, $\mathcal{F}_i^2$(ZM) and $\mathcal{F}_i^2$(MQ), are

$$\mathcal{F}_i^2(ZM) = \sin(\pi J_i \tau_2) \exp[-(R_2^{I_i} + \tfrac{1}{2}R_{1**}^{S_i})\tau_2] \times \exp(-R_1^{I_i}\tau_3) \quad (8)$$

$$\mathcal{F}_i^2(MQ) = \sin(\pi J_i \tau_3) \exp[-(R_2^{I_i} + \tfrac{1}{2}R_{1**}^{S_i})\tau_3] \times \exp(-R_{MQ}^{I_i S_i}\tau_2) \cos^{n-1}(\pi J_i \tau_2), \quad (9)$$

where $R_{MQ}^{I_i S_i}$ represents the relaxation rate for the double/zero quantum coherence $2I_y^i S_x^i$. Using further phase cycling (Akke et al., 1994) or pulse gradient pathway selection (Muhandiram and Kay, 1993) to balance the two pathways and therefore cancel the mirror-image peaks, the extended reverse INEPT transfer amplitude for both echo and anti-echo signal is

$$\mathcal{F}_i^2 = \mathcal{F}_i^2(ZM) + \mathcal{F}_i^2(MQ) \quad (10)$$

From Equations (8)–(10), it can be seen that, in a sensitivity-enhanced experiment, the 3D NOE cross peak intensity is further modulated by, in addition to relaxation effects, passive J-coupling modulation for CH_2 and CH_3 moieties for the MQ coherence pathway. To avoid these complications, the sensitivity-enhancement scheme is usually not employed in structure refinement, despite the fact that it can increase the overall sensitivity up to 20–70% (Schleucher et al., 1994). However, if these effects are properly taken into account in back-calculation, the sensitivity-enhanced NOESY-HSQC experiment could then be used in direct structure refinement.

Combining the effects discussed above, the final NOESY-HSQC cross-peak intensity for the transfer pathway $I_z^j \longrightarrow I_z^i \longrightarrow 2I_z^i S_{x,y}^i \longrightarrow I_{x,y}^i$ can be obtained as

$$I_{ij} = M_z^j(0)[\exp(-\mathbf{R}t_m)]_{ij}\mathcal{F}_i, \quad (11)$$

where $M_z^j(0)$ can be calculated by Equation (3) or (4). $\mathcal{F}_i = \mathcal{F}_i^1 \mathcal{F}_i^2$, the overall editing efficiency through spin S_i. $\mathcal{F}_i^2$ can be calculated using Equation (7) for a conventional NOESY-HSQC experiment, or using Equation (10) for a sensitivity-enhanced experiment, as discussed above. Equation (11) shows that $I_{ij} \neq I_{ji}$, because $\mathcal{F}_i \neq \mathcal{F}_j$ and $M_z^j(0) \neq M_z^i(0)$. As described above, in a sensitivity-enhanced experiment, the difference between $\mathcal{F}_i$ and $\mathcal{F}_j$ can be large simply because spin i and spin j belong to different CH_n groups. From Equation (10), neglecting relaxation, it can be calculated that the intensity ratio of the C^iH^i-$C^jH_3^j$ cross peak in the C^i plane to the $C^jH_3^j$-C^iH^i cross peak in the C^j plane is $\sim 1.7 : 1.2$, provided that $\tau_1 = \tau_3 = 1/2J_{CH}$, $\tau_2 = 1/4J_{CH}$, and that $M_z^j(0) = M_z^i(0)$. The values of $M_z^j(0)$ and $M_z^i(0)$ differ significantly when the relaxation delay is not long enough and spin i and spin j have different longitudinal relaxation rates, for example, when protons in labeled residues and in unlabeled residues are involved.

Calculation of the relaxation matrix

The relaxation matrix for the Solomon equation can be calculated as

$$(\mathbf{R})_{ij} = \frac{\gamma_H^4\hbar^2}{10}[6J^{ij}(2\Omega_H) - J^{ij}(0)] \quad (12)$$

$$\begin{aligned}(\mathbf{R})_{ii} &= \frac{\gamma_H^4\hbar^2}{10}\sum_{j\neq i}^{n}[J^{ij}(0) + 3J^{ij}(\Omega_H) \\ &+ 6J^{ij}(2\Omega_H)] \\ &+ \sum_S \frac{\gamma_H^2\gamma_S^2\hbar^2}{10}\sum_{k_S}[J^{ik_S}(\Omega_H - \Omega_S) \\ &+ 3J^{ik_S}(\Omega_H) + 6J^{ik_S}(\Omega_H + \Omega_S)] \\ &+ R_i^{ext}, \end{aligned} \quad (13)$$

where i and j represent two protons, and k_S is a heteronuclear spin of type S in the labeled sample. R_i^{ext} is the external relaxation rate for spin i, representing the interactions with further spins not included in the calculation, or errors due to the imperfection of the theoretical treatment. $J^{ij}(\Omega)$ is the spectral density for the vector connecting spin i and spin j. For a rigid **ij** vector in a molecule tumbling as a symmetric top,

$$J^{ij}(\Omega) = \frac{4\pi}{5}\sum_{n=-2}^{2}\frac{\tau_n}{1+\Omega^2\tau_n^2}\frac{|Y_{2n}(\Phi_{ij})|^2}{r_{ij}^6} \quad (14)$$

$$\tau_n^{-1} = 6D_\perp + n^2(D_\parallel - D_\perp), \quad (15)$$

where $\Phi_{ij} = (\theta_{ij}, \phi_{ij})$ are the polar angles made by **ij** in a principal axis system of the symmetric top; Y_{2n} is the spherical harmonics; $D_\parallel$ and $D_\perp$ are the rotational diffusion constants parallel and perpendicular to the symmetry axis.

When internal motions are involved, the above equation needs to be modified. A general approach has been described by Tropp (1980), in which the internal motion was treated as an N-site jump. Below, two special cases, where the internal motional correlation time is much faster or slower than the overall tumbling correlation time, are described. These results can be easily deduced from the general equation of Tropp's original paper (Equation (14.2), Tropp, 1980). For the isotropic case, the results have been described by Yip and Case (1991), and the effect of the slow flip of an aromatic ring and that of the fast rotation of a methyl group on the NOE intensity have been demonstrated by Liu et al. (1992) and Olejniczak and Weiss (1990).

Slow internal motion

When internal motion is much slower than the overall molecular tumbling, it can be shown that the spectral density is independent of the internal motional rates,

$$J^{ij}(\Omega) = \frac{4\pi}{5}\sum_{n=-2}^{2}\frac{\tau_n}{1+\Omega^2\tau_n^2}\left\langle\frac{|Y_{2n}(\Phi_{ij})|^2}{r_{ij}^6}\right\rangle, \quad (16)$$

where $\langle\cdots\rangle$ represents a conformational average. Equation (16) indicates that the relaxation matrix elements (Equations (12) and (13)) for a molecule undergoing slow internal motions between multiple conformations can be simply obtained by averaging the relaxation matrix elements calculated from these conformers as rigid molecules.

Fast internal motion

When internal motion is much faster than the overall tumbling, within the strong narrowing limit (Hoffman, 1970; Zhu, 1996), the *homonuclear* zero-quantum spectral density $J^{ij}(\Omega_H^i - \Omega_H^j) \approx J^{ij}(0)$ can also be shown to be independent of the internal jumping rates,

$$J^{ij}(\Omega) = \frac{4\pi}{5}\sum_{n=-2}^{2}\frac{\tau_n}{1+\Omega^2\tau_n^2}\left|\left\langle\frac{Y_{2n}(\Phi_{ij})}{r_{ij}^3}\right\rangle\right|^2, \quad (17)$$

where $\Omega = \Omega_H^i - \Omega_H^j$, and $(\Omega_H^i - \Omega_H^j)\tau_n \ll 1.0$. However, it must be pointed out that, in biomolecular systems with long correlation times, for all the other spectral densities, $J(\Omega_H)$, $J(2\Omega_H)$, and $J(\Omega_H - \Omega_S)$, etc., Equation (17) is generally incorrect and these spectral densities are explicitly dependent on the internal motional rates (Tropp, 1980). As long as $J^{ij}(0) \gg J^{ij}(2\Omega_H)$, or $(\mathbf{R})_{ij} \approx -(\gamma_H^4\hbar^2/10)J^{ij}(0)$, the cross-relaxation rate can be calculated with reasonable accuracy by using Equation (17) to account for the fast internal motions. On the other hand, errors are introduced in calculating the longitudinal relaxation rates, $T_{1i}^{-1} = (\mathbf{R})_{ii} + \sum_{j\neq i}^{n}(\mathbf{R})_{ij}$. If the internal motional correlation times are not available, the error introduced can only be corrected by incorporating it into the empirical external relaxation rate, R_i^{ext}.

From Equation (17), it can be seen that, for fast internal motion, in contrast to the situation where internal motion is slow, the distance dependence of the NOE intensity is averaged over r^{-3} instead of r^{-6}. The conformational average over $Y_{2n}(\Phi_{ij})$, instead of over $\left|Y_{2n}(\Phi_{ij})\right|^2$ as in the slow internal motion case (Equation (16)), also has a significant effect by scaling down the spectral density. Generally, a reliable dynamic trajectory is required (to obtain the relative populations along the trajectory) to calculate $J^{ij}(0)$ and $(\mathbf{R})_{ij}$. However, if the fast internal motion can be considered as jumping among equivalent sites (such as the three-site jump of a methyl group), and if the conformation of the obtained structure represents one of these sites, the calculation is rather simple.

The NOESY-HSQC simulation program SPIRIT

Calculation method

Equation (11) is the basis for the NOESY-HSQC simulation program SPIRIT. $M_z^j(0)$ is calculated using Equation (3). For the calculation of spectral densities and the relaxation matrix, the molecule is generally treated as rigid. However, the fast rotation of methyl groups are explicitly taken into account by using Equation (17), assuming the three-site jump motional model (or nine-site jump model for methyl–methyl interactions) and that the input conformation represents one of the equivalent sites. To consider slow internal motions, the program allows input of multiple conformations (as PDB files) together with information on their relative populations; average values of the spectral densities and the relaxation matrix are calculated using Equation (16). To calculate the exponent $\exp(-\mathbf{R}t_m)$, the relaxation matrix $\mathbf{R}$ was diagonalized by consecutive use of Householder reduction and QL algorithms (Press et al., 1989).

Theoretically, $\mathcal{F}_i = \mathcal{F}_i^1\mathcal{F}_i^2$ can be calculated using Equations (6) and (7) or (10), provided that all of the relevant relaxation rates can be experimentally determined or theoretically calculated, which is not always an easy task. Practically, since the relative magnitude of $\mathcal{F}_i$ is proportional to the corresponding cross-peak intensity of the 2D HSQC experiment, $\mathcal{F}_i$ can be obtained by measuring the cross-peak intensity in an HSQC experiment which employs the same experimental parameters as in the NOESY-HSQC experiment, except that the relaxation delay in the HSQC experiment should be long enough to ensure equal z magnetization recoveries. This approach can be used if the HSQC spectrum is well resolved. However, if the corresponding 2D HSQC spectrum is not well resolved, as for most ^{13}C HSQC spectra of medium size proteins, the above method appears impractical. In such a case, the editing efficiencies are calculated by neglecting relaxation in Equations (6) and (7) or (10), i.e.,

$$\mathcal{F}_i = \sin(\pi J_i\tau_1)\sin(\pi J_i\tau_2), \tag{18}$$

or, if the sensitivity enhancement scheme is used,

$$\mathcal{F}_i = \sin(\pi J_i\tau_1)[\sin(\pi J_i\tau_2)+ \\ +\sin(\pi J_i\tau_3)\cos^{n-1}(\pi J_i\tau_2)]. \tag{19}$$

Equations (18) and (19) are valid if the proton T_2 is longer than $5\tau_1$ ($\sim$18.5 ms for $\tau_1 = 3.7$ ms). For proteins or protein complexes of size < 30 kDa, the proton T_2 is in general longer than $5\tau_1$ except when slow internal motions are involved or when aggregation is significant.

Therefore, to meet different needs in differing situations, two versions of SPIRIT have been written. Version 1 (SPIRIT1) uses the relative intensity of the corresponding HSQC cross peaks as the editing efficiencies, which can be applied where the HSQC spectrum is reasonably resolved. Version 2 (SPIRIT2) calculates the editing efficiencies using Equations (18) or (19). Generally, SPIRIT1 is more suitable for ^{15}N NOESY-HSQC spectral simulations, while SPIRIT2 is more suitable for ^{13}C NOESY-HSQC spectral simulations.

Input files

PDB files. The programs need one or more PDB files for coordinate information. Currently, the standard Brookhaven PDB files and PDB files produced by DISCOVER and by AMBER are acceptable.

PPM file. The information on chemical shifts, linewidths, external relaxation rates, and one-bond connectivity, among others, is included in the PPM file. A representative example of a PPM file extract is shown in Figure 1.

In Figure 1, parts ①-③ constitute the header part of a PPM file. Part ① gives basic experimental and processing parameters in each dimension, such as spectral frequencies (#freq, in MHz), spectral widths (#spwd, in Hz), spectral size (#size, in points), reference points and their corresponding chemical shift

```
!A sample PPM file.
!Lines starting with a "!" are comments.

!          D1        D2        D3
!---->!-------->!-------->!-------->
#freq:    600.13    600.13    150.91
#spwd:   7183.9    7183.9    5555.6
#size:       512       256       128
#rfpt:     187.0     169.0      49.0
#rfpm:      4.22      3.13      42.8
#lwfc:       1.0      2.38       1.0

!unlabeled residues:
!a12         a5   a5   a5   a5   a5
!---------->!--->!--->!--->!--->!--->
#unlabled:        87   88   89   90
#unlabled:  91   92   93   94   95
......

!methyl groups in unlabeled residues.
!a8        a5   a5   a5   a5
!------>!--->!--->!--->!--->
#rotor: 92   H71  H72  H73
#rotor: 93   H71  H72  H73
#rotor: 94   H71  H72  H73
......
!--->!--->!--->!------>!------>!------>!------>
15   LYS  N        116.7    70.0    94.0   H
15   LYS  CA        56.6   150.0   142.0   HA
15   LYS  CB        29.5   150.0   120.0   HB[23]
15   LYS  CG        21.9   150.0   120.0   HG[23]
15   LYS  CD        26.7   150.0   120.0   HD[23]
15   LYS  CE        39.3   150.0   120.0   HE[23]
15   LYS  H         7.35    38.0     0.5    3.2
15   LYS  HA        3.80    38.0     0.5    2.8
15   LYS  HB2       1.80    38.0     0.5    2.3
15   LYS  HB3       1.80    38.0     0.5    2.2
15   LYS  HG2       1.44    38.0     0.5    2.2
15   LYS  HG3       1.33    38.0     0.5    2.2
15   LYS  HD2       1.53    38.0     0.5    2.5
15   LYS  HD3       1.53    38.0     0.5    2.6
15   LYS  HE2       2.88    38.0     0.5    2.3
15   LYS  HE3       2.88    38.0     0.5    2.3
......

92   DT   H1'      6.325    30.0     0.5
92   DT   H2'2     2.268    30.0     0.5
92   DT   H2'1     1.898    30.0     0.5
92   DT   H3'      5.022    30.0     0.5
92   DT   H4'      3.676    30.0     0.5
92   DT   H5'1  -999.99     30.0     0.5
92   DT   H5'2  -999.99     30.0     0.5
92   DT   H6       7.334    30.0     0.5
92   DT   H71      2.028    30.0     0.5
92   DT   H72      2.028    30.0     0.5
92   DT   H73      2.028    30.0     0.5
......
```

Figure 1. An example PPM file extract for the 3D NOESY-HSQC program SPIRIT on a protein–DNA complex.

values (#rfpt in point and #rfpm in ppm, respectively), and a multiplying factor for linewidth in each dimension (#lwfc), which is necessary since the proton resonance linewidths are generally different in the D1 (t_3) and D2 (t_1) dimensions. Part ② indicates the unlabeled residues, which, in the example given, are the DNA residues in a protein–DNA complex. Part ③ identifies the fast-rotating methyl groups in unlabeled residues. Methyl groups in labeled residues can be distinguished by SPIRIT1 and SPIRIT2. Parts ② and ③ can be skipped if the sample contains no unlabeled residues.

Parts ④–⑥ represent the main body of a PPM file. In the present example, parts ④ and ⑤ give the information on residue 15, which is a ^{13}C, ^{15}N double-labeled lysine. Part ⑥ gives the information on residue 92, which is an unlabeled deoxythymine.

Part ④ provides chemical shifts (in ppm), linewidths (in Hz) of heteronuclei, one-bond J-coupling constants, and the directly bonded protons. If several protons are attached to the heteronucleus, these are represented by their common name followed by their indices within a bracket. For example, HB2 and HB3 are represented by HB[23]. Part ⑤ provides chemical shifts, linewidths, external relaxation rates (in s^{-1}), and heteronuclear editing efficiencies with respect to these protons, which are the relative intensities of the corresponding HSQC spectrum. For the program SPIRIT1, the information inside the shaded boxes is not necessary, and can be left blank. For the program SPIRIT2, on the other hand, the information inside the unshaded boxes is extraneous, and can be left blank; the editing efficiencies are calculated using Equations (18) or (19). Part ⑥ gives chemical shifts, linewidths and external relaxation rates of the unlabeled residues.

An auxiliary program, MAKEPPM, has been written to prepare the PPM file from a protein or nucleic acid sequence. The actual chemical shifts, linewidths, etc., are to be provided by the user.

Interactive input. Options to treat the molecular tumbling mode as isotropic or as anisotropic, correlation time(s), mixing time(s), the duty cycle, information as to whether the sample is double-labeled or just ^{13}C- or ^{15}N-labeled, and for SPIRIT2, whether the experiment is a conventional NOESY-HSQC or a sensitivity-enhanced one, and corresponding coherence transfer delays, are input interactively.

Viewing the simulated spectra

It is useful to view the simulated spectra to compare them with the experimental data, especially in regions where peaks are overlapped; some obvious errors in the interim structures can then be identified. For example, if a rather strong NOE peak occurs in the simulated spectrum which is absent from the experimental spectrum, a lower bound for the two protons giving rise to the NOE peak can be justified.

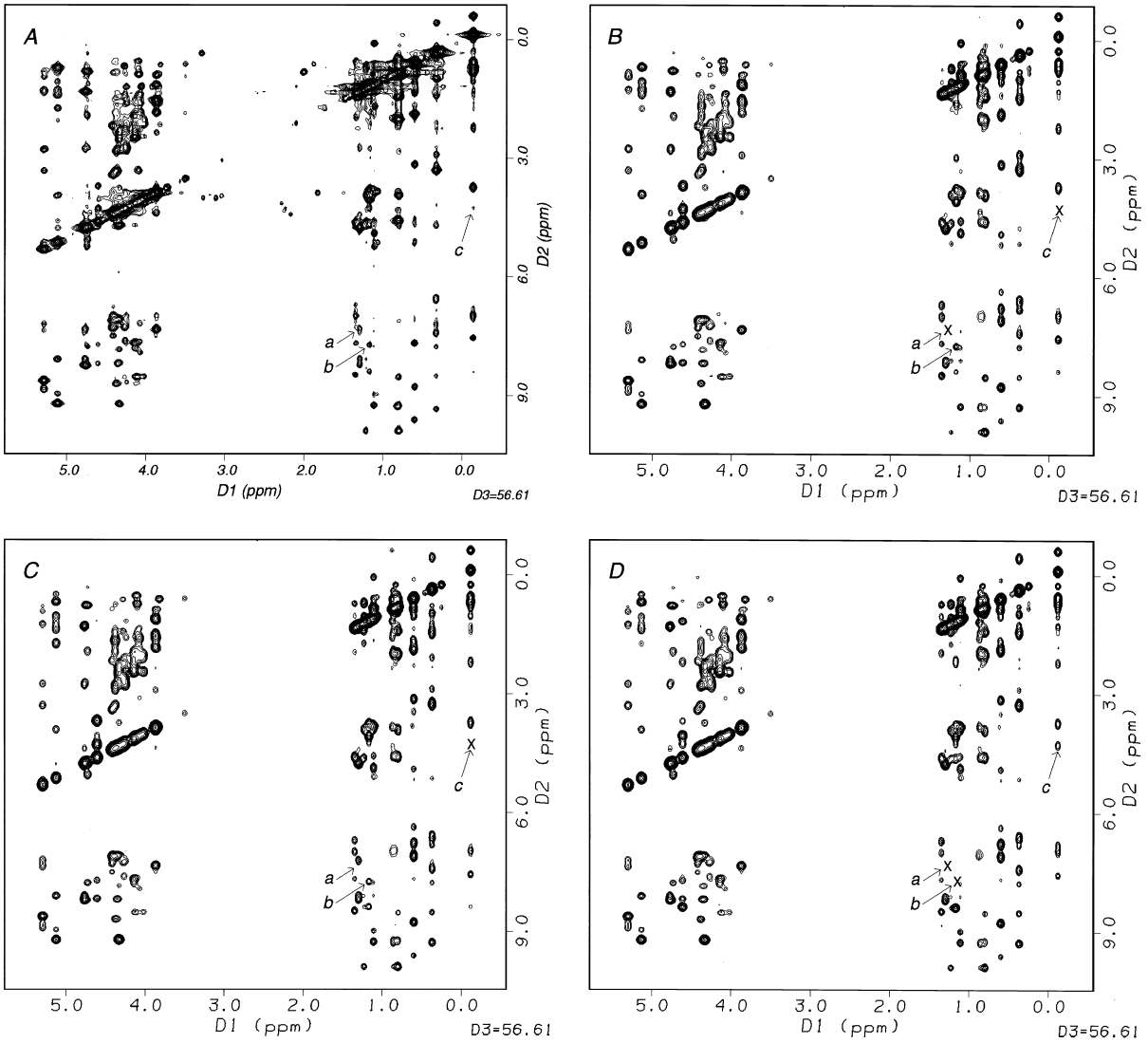

Figure 2. D1-D2 planes at ^{13}C chemical shifts of 56.61 ppm and 19.79 ppm (folded) of the NOESY-HSQC spectrum at 160 ms mixing time. (A) Experimental spectrum; (B) simulated spectrum from NMR structures; (C) simulated spectrum from molecule A of the two X-ray crystal structures; and (D) simulated spectrum from molecule B of the two X-ray crystal structures. Peak 'a' represents the NOE between Thr8 MG2 and His6 HD2; peak 'b' represents the NOE between Thr14 MG2 and Thr14 HN; peak 'c' represents the NOE between Val16 MG2 and Ser11 HB1. When a peak is missing, it is represented by an 'x'.

After obtaining an NOE intensity file from SPIRIT1 or SPIRIT2, the program MAKE3D can be used to calculate the 3D matrix, which can be loaded into a FELIX (Molecular Simulation, Inc.) matrix file and viewed in FELIX. The chemical shift and linewidth information in the PPM file is not necessary for calculating cross-peak intensities, but is only relayed to the NOE intensity file and is used by MAKE3D.

Application of SPIRIT

The SPIRIT program has been tested on the oxidized *E. coli* thioredoxin, which contains 108 amino acid residues. Both the X-ray crystal structure (Katti et al., 1990) and high-resolution NMR structures (Jeng et al., 1994) of the protein have been reported.

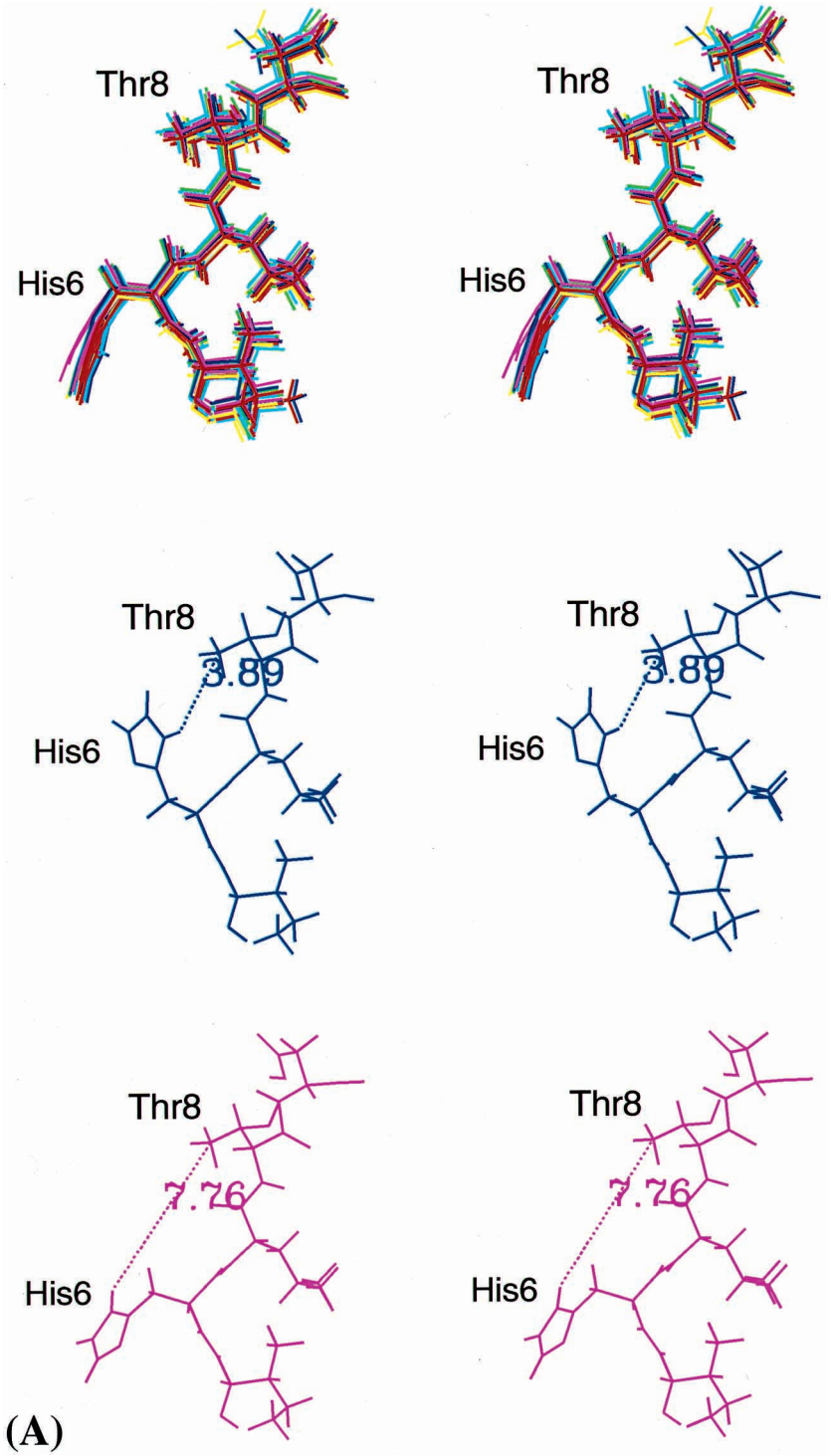

Figure 3. (A) The conformation of the segment Ile5-His6-Leu7-Thr8-Asp9 of the oxidized *E. coli* thioredoxin for the superimposed 20 NMR structures (upper), for molecule A of the two X-ray crystal structures (middle), and for molecule B of the two X-ray crystal structures (bottom). The distance between Thr8 CG2 and His6 HD2 is shown in molecule A and molecule B; this distance is 8.5 ± 0.1 Å in the 20 NMR structures.

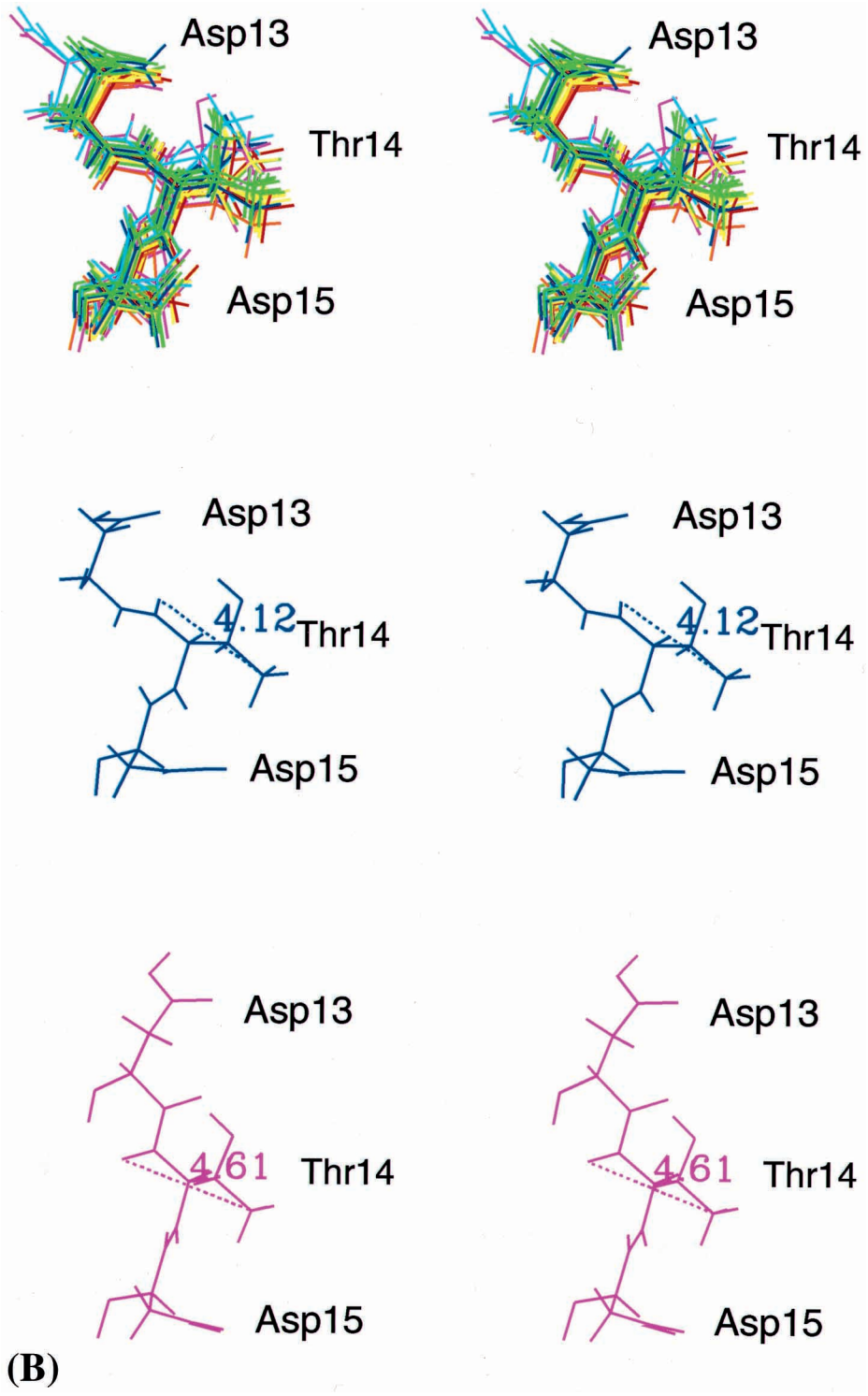

Figure 3. (B) The conformation of the segment Asp13-Thr14-Asp15 of the oxidized *E. coli* thioredoxin for the superimposed 20 NMR structures (upper), for molecule A of the two X-ray crystal structures (middle), and for molecule B of the two X-ray crystal structures (bottom). The distance between Thr14 CG2 and Thr14 HN is shown in molecule A and molecule B; this distance is 3.6 ± 0.4 Å in the 20 NMR structures.

Acquisition of NOESY-HSQC spectra

Two ^{13}C NOESY-HSQC spectra (mixing times: 80 ms and 160 ms) of the oxidized *E. coli* thioredoxin in 10%D_2O:90%H_2O were acquired on a Bruker DRX600 spectrometer at 308 K. The spectral widths were 11.97 ppm, 11.97 ppm and 36.53 ppm in the D1 (t_3), D2 (t_1) and D3 (t_2) dimensions, with the carrier at 2.61 ppm, 5.05 ppm and 38.5 ppm, respectively. Sensitivity-enhancement (Cavanagh et al., 1991; Palmer et al., 1991) was used. The INEPT delay (τ_1), reverse INEPT delay (τ_2), and multiple quantum coherence recovery delay (τ_3) were 3.66, 1.83 and 3.66 ms, respectively. The duty cycle (i.e., relaxation delay + acquisition time) was 1.25 s. A data set containing 512, 128 and 46 complex points in the D1(t_3), D2(t_1) and D3(t_2) dimensions, respectively, was acquired. Further zero-filling during data processing resulted in a final matrix of dimensions $512\times256\times128$. A D1-D2 plane at ^{13}C chemical shifts of 56.61 ppm and 19.79 ppm (folded) of the NOESY-HSQC spectrum at 160 ms mixing time is shown in Figure 2A.

Spectral simulation using SPIRIT

Because the ^{13}C HSQC spectrum of the protein is rather crowded, it would be difficult to measure the intensities of the HSQC spectrum for many protons to estimate their ^{13}C-editing efficiencies. Therefore, we decided to use SPIRIT2 to simulate these ^{13}C NOESY-HSQC spectra, in which the ^{13}C-editing efficiencies are calculated using Equation (19). The CPU time for the simulation (from a single structure, consisting of 769 protons, 528 carbons and 132 nitrogens) is ∼13 min on an SGI O^2 (MIPS R5000, 180 MHz IP32 processor, 128 Mb RAM), or ∼29 min on an SGI Indy (MIPS R4600, 133 MHz IP22 processor, 96 Mb RAM).

The correlation time used in the simulation is 6.41 ns, which has been determined previously from ^{15}N relaxation measurements for the oxidized *E. coli* thioredoxin in a similar buffer and at the same temperature (Stone et al., 1993). All other parameters used in the simulation are the same as those used in the experiment, i.e., $\tau_1 = \tau_3 = 3.66$ ms, $\tau_2 = 1.83$ ms, RD + AQ = 1.25 s. Rigorously, the external relaxation rates, R_i^{ext}, should be determined individually, which can be accomplished by fitting the proton longitudinal magnetization recovery curves (Zhu and Reid, 1995). However, this approach is only practical for those protons which are resolved in the HSQC spectrum such that their M_z recovery curves can be experimentally determined. It was found that the R_i^{ext} values of ∼0.6 s^{-1} (∼0.75 s^{-1} for methyl groups) fit the M_z recovery curves reasonably well for protons whose HSQC peaks are resolved. (Proton M_z recovery curves were measured by a series of HSQC experiments which were preceded by a variable delay (M_z recovery time) after proton presaturation – data not shown.) Under these simulation conditions, the range of editing efficiencies is 1.21–1.73. The variation is mainly due to the passive coupling modulation on CH_n, as well as variations in one-bond J-coupling constants. The range of proton M_z recoveries is relatively uniform for the present case, ∼0.67–0.75. However, M_z recoveries can differ significantly in cases where some protons are rather isolated, such as the H2 protons in DNA (Zhu and Reid, 1995), or when the sample is partially labeled; in such a case, protons of the labeled residues would relax significantly faster than those of the unlabeled residues due to the strong one-bond dipolar interaction.

For the spectral simulation using the NMR coordinates (Jeng et al., 1994), the relaxation matrix was averaged over 20 structures, with a relative population of 1.0 for all the structures. Figure 2B shows a D1–D2 plane of the simulated spectrum with mixing time $t_m = 160$ ms at the same ^{13}C chemical shift as shown in Figure 2A. The agreement between the simulated spectra and experimental ones is striking, an indication that the family of NMR structures is well fitted to the NMR data. For comparison, a simulation was also performed using the X-ray crystal structure of the oxidized thioredoxin. There are two molecules, which will be referred to as molecule A and molecule B in the following discussion, in the asymmetric unit (Katti et al., 1990); while the structures of the two molecules are very similar overall, some differences in local conformation are observed due to differences in crystal packing. The D1–D2 planes at the same ^{13}C chemical shift as in Figures 2A and 2B are shown in Figure 2C for molecule A and in Figure 2D for molecule B; the spectra for each of the X-ray conformers were simulated with mixing time $t_m = 160$ ms.

Comparing Figures 2B, 2C and 2D with Figure 2A, it can be seen that the spectra simulated from the set of NMR structures and the two X-ray crystal structures agree quite well with each other and with the experimental spectrum. However, some deviations can also be found and some interesting differences between the three simulated spectra are observed. Following are some examples. A medium size cross peak (indicated

by an 'a') in the experimental NOESY spectrum is totally absent from the simulated spectrum for molecule B as shown in Figure 2D. Peak 'a' represents the NOE between Thr8 MG2 and His6 HD2. This peak is also absent from the spectrum simulated from the NMR structures (Figure 1B), but is present in the simulated spectrum for X-ray molecule A (Figure 2C). The above observations can be correlated with local structural features (Figure 3A). From Figure 3A, it can be seen that, in terms of His6 side-chain configuration, the NMR structures are similar to molecule B, but different from molecule A. The distance between Thr8 CG2 and His6 HD2 is 3.9 Å in molecule A, close enough to give an NOE peak between Thr8 MG2 and His6 HD2 in the simulated spectrum (Figure 2C). This distance is 7.8 Å in molecule B and 8.5 $\pm$ 0.1 Å in the NMR structures, and therefore the NOE between Thr8 MG2 and His6 HD2 is absent from the simulated spectra (Figures 2D and 2B). Since this cross peak is present in the experimental spectrum (Figure 2A), the structure of molecule A is more consistent with the NMR data if a rigid model is assumed. However, since the His6 side chain is on the surface of the protein, it is very likely that the imidazolyl ring is actually conformationally averaged through rotation about the χ_1 and χ_2 dihedral angles. Evidence for such conformational averaging in His6 side chain conformation was previously observed at higher temperatures (Jeng et al., 1994).

Peak 'b', which represents the intra-residue MG2-HN NOE in Thr14, is also absent from the simulated spectrum for X-ray molecule B (Figure 2D). However, this peak is observed in the spectra simulated for the NMR structures (Figure 2B) and for molecule A (Figure 2C), and is also present in the experimental NOESY spectrum (Figure 2A). This observation is consistent with the fact that the family of the 20 NMR structures is locally similar to the structure of molecule A at the segment Asp13-Thr14-Asp15, as shown in Figure 3B. The distance between Thr14 CG2 and Thr14 HN is 4.1 Å in molecule A and 3.6 $\pm$ 0.4 Å in the NMR structures; in molecule B, this distance is 4.6 Å, which means that the methyl protons are more than 5 Å from the amide proton and consequently do not give rise to an NOE. Therefore, it seems that the NMR structures and molecule A are more consistent with the NMR data than molecule B.

If the simulated spectra are analyzed and compared to the experimental ones in a quantitative way, detailed information about the consistency of the interim structures with the experimental NOE data can be obtained. For example, the furthest upfield resonance in Figures 2A–2D comes from the MG2 methyl group of Val16. To compare more quantitatively the simulated spectra for the NMR solution structures and for the X-ray crystal structures with the experimental spectrum, the D2 slices corresponding to the Val16 MG2 resonance in Figures 2A–2D are aligned, as shown in Figure 4. It can be seen from Figure 4 that, for most peaks, the intensity of the simulated spectra agrees quite well with that of the experimental spectrum. However, intensity deviations can be observed for some peaks. For example, peak 'c' in Figure 2 and Figure 4 represents the NOE between Val16 MG2 and Ser11 HB1, which is very weak in the experimental spectrum. However, this peak is quite strong in the simulated spectrum for molecule B (which has a Val16 CG2–Ser11 HB1 distance of 3.4 Å), but is completely absent from the simulated spectra for molecule A (which has a Val16 CG2–Ser11 HB1 distance of 8.6 Å) and for the NMR structures (which have a Val16 CG2–Ser11 HB1 distance of 7.0 $\pm$ 0.3 Å). It has yet to be determined whether the low intensity of peak 'c' in the experimental NOESY-HSQC spectrum reflects the presence of a rigid structure that is different from either X-ray molecule A or molecule B (or the NMR structures), or whether it reflects conformational averaging in solution that includes both X-ray conformations.

The sensitivity of the simulated spectra to local differences in conformation, as demonstrated by the examples given above, holds promise that differences in cross-peak intensity between experimental and simulated spectra could be used to check the consistency of NMR-derived structures with the experimental NOE data, as well as to refine NMR structures.

Discussion and Conclusions

The NOESY-HSQC simulation program SPIRIT described in this paper has the following features: (a) it takes into account differences in transfer efficiency during the INEPT and reverse INEPT processes due to differential relaxation rates and ^1J coupling constants; (b) it considers differing effects of the sensitivity-enhancement scheme on CH, CH_2 and CH_3 moieties, so that sensitivity-enhanced experiments can be used in structure refinement; (c) it accounts for incomplete and differential recovery of longitudinal magnetization between scans when an insufficiently long relaxation delay is used, a particular problem in 3D

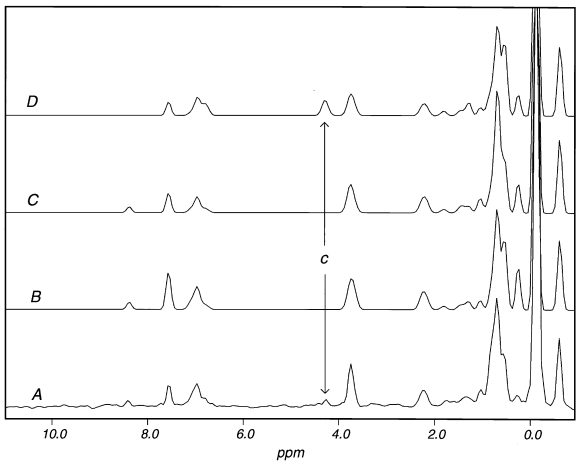

Figure 4. D2 slices from Figure 2A–2D at −0.12 ppm (corresponding to the resonance of Val16 MG2), illustrating the magnitude of the intensity differences for certain cross peaks between experimental and simulated spectra. (A) Experimental spectrum; (B) simulated spectrum from NMR structures; (C) simulated spectrum from molecule A of the two X-ray crystal structures; and (D) simulated spectrum from molecule B of the two X-ray crystal structures. As in Figure 2, peak 'c' is the NOE interaction between Val16 MG2 and Ser11 HB1.

experiments. This feature is very useful if the sample is partially labeled, such as in a protein–DNA complex where the protein is labeled with ^{13}C and ^{15}N while the DNA is unlabeled; in such a system, the proton longitudinal relaxation times of the labeled residues are significantly shorter than those of the unlabeled residues due to the strong one-bond dipolar interaction; (d) some well-defined internal motions, such as the fast rotation of methyl groups, are explicitly taken into account; methyl groups usually occur in large number in proteins and constraints to methyl groups play important roles in structure determination; and (e) the program allows for input of multiple conformations together with information on their relative populations to make it possible to consider slow motions among multiple conformations; the relaxation matrix is then averaged over these conformations. However, it must be pointed out that it is often difficult to distinguish whether the multiple conformers observed in NMR structures truly reflect real internal motion, or simply result from insufficient restraints. For the structural divergence simply due to insufficient restraints, such an averaging scheme, although not physically meaningful, provides a method to show how the ensemble of these structures agrees with the available NOE data.

Our ultimate goal is to use the simulation program to automatically refine NMR-based biomolecular structures, which can be accomplished by two methods. One is the (NOE) gradient-based direct structure refinement, which can be incorporated into molecular dynamics routines (Yip and Case, 1989; Yip, 1993). The other is the distance restraint-based indirect method (Boelens et al., 1989; Borgias and James, 1990; Post et al., 1990; Kim and Reid, 1992). In this method, after obtaining interim structures, the simulated NOE intensities can be calculated. By comparing the simulated NOE intensities with the experimental ones, a current NMR R-factor can be calculated, and a new restraints file can be produced; improved structures can then be obtained using the improved restraints. This process should be repeated iteratively until a satisfactory agreement between simulated and experimental spectra is obtained. The first method is mathematically more elegant and development of the methodology is still in progress. However, the second method is intuitively simpler. Furthermore, distance restraints are necessary for distance geometry calculation; more accurate and narrower restraints greatly facilitate the conformation search, especially at the beginning stage of structure determination when the number of unambiguous restraints is limited.

The occurrence of internal motion always presents a challenge in NMR-based structure determination. The effect of internal motion on the spectral density and NOE intensity depends on the time scale, as described above. Heteronuclear relaxation studies may provide important information on this matter. For internal motion much faster than overall tumbling, the model-free approach (Lipari and Szabo, 1982a, b) can be used to determine the generalized order parameter $\mathcal{S}$ and effective correlation time τ_e by fitting the T_1, T_2 and ^{15}N{^{1}H} or ^{13}C{^{1}H} NOE data. If internal motions with correlation times comparable to the overall tumbling correlation time are involved, more parameters describing these slower internal motions need to be included in the fitting (Clore et al., 1990). Internal motions much slower than the overall tumbling result in shorter T_2 and line broadening, since the chemical exchange contribution to T_2 becomes significant in such a case. Measurement of $T_{1\rho}$ can be useful for estimating the exchange rate (Jones, 1966; Wang, 1992). Information on internal motions must be carefully considered in structural refinement using NOESY-HSQC simulation. Since, except for methyl groups, the SPIRIT programs treat the molecules as rigid, deviations of simulated NOE intensities from

the experimental data should be tolerated to some extent when relaxation data indicate fast internal motions involving protons participating in the NOE transfer. Development of methods to quantitatively utilize the simulated NOESY-HSQC data in structure refinement is in progress.

The programs SPIRIT1, SPIRIT2, MAKEPPM and MAKE3D are available from the authors upon request. These programs are coded in standard FORTRAN77, and are quite portable on different platforms.

Acknowledgements

The authors thank Dr David Case for helpful discussions and Dr John Chung for technical assistance in NMR data acquisition. This work was supported by grants GM36643 and GM43238 from the National Institutes of Health.

References

Akke, M., Carr, P.A. and Palmer, A.G. (1994) *J. Magn. Reson.*, **B104**, 298–302.

Bax, A. (1989) *Curr. Opin. Struct. Biol.*, **4**, 738–744.

Boelens, R., Koning, T.M.G., van der Marel, G.A., van Boom, J.H. and Kaptein, R. (1989) *J. Magn. Reson.*, **82**, 290–308.

Borgias, B.A. and James, T.L. (1990) *J. Magn. Reson.*, **87**, 475–487.

Cavanagh, J., Palmer, A.G., Wright, P.E. and Rance, M. (1991) *J. Magn. Reson.*, **91**, 429–436.

Cavanagh, J., Fairbrother, W.J., Palmer, A.G. and Skelton, N.J. (1996) *Protein NMR Spectroscopy*, Academic Press, San Diego, CA.

Chandrasekhar, K., Krause, G., Holmgren, A. and Dyson, H.J. (1991) *FEBS Lett.*, **284**, 178–183.

Chandrasekhar, K., Campbell, A. P., Jeng, M. F., Holmgren, A. and Dyson, H.J. (1994) *J. Biomol. NMR*, **4**, 411–432.

Clore, G.M. and Gronenborn, A.M. (1989) *Crit. Rev. Biochem. Mol. Biol.*, **24**, 479–564.

Clore, G.M., Driscoll, P.C., Wingfield, P.T. and Gronenborn, A.M. (1990) *Biochemistry*, **29**, 7387–7401.

Dyson, H.J., Holmgren, A. and Wright, P.E. (1989) *Biochemistry*, **28**, 7074–7087.

Görler, A. and Kalbitzer, H.R. (1997) *J. Magn. Reson.*, **124**, 177–188.

Hoffman, R.A. (1970), *Adv. Magn. Reson.*, **4**, 87–200.

Ikura, M., Kay, L.E. and Bax, A. (1990) *Biochemistry*, **29** 4659–4667.

Jeng, M.-F., Campbell, A. P., Begley, T., Holmgren, A., Case, D., Wright, P.E. and Dyson, H.J. (1994) *Structure*, **2**, 853–868.

Jones, G.P. (1966) *Phys. Rev.*, **148**, 332–335.

Katti, S.K., LeMaster, D.M. and Eklund, H. (1990) *J. Mol. Biol.*, **212**, 167–184.

Kay, L.E., Ikura, M., Tschudin, R. and Bax, A. (1990) *J. Magn. Reson.*, **89**, 496–514.

Kim, S. and Reid, B.R. (1992) *J. Magn. Reson.*, **100**, 382–390.

Köck, M. and Griesinger, C. (1994) *Angew. Chem., Int. Ed. Engl.*, **33**, 332–334.

Lipari, G. and Szabo, A. (1982a) *J. Am. Chem. Soc.*, **104**, 4546–4559.

Lipari, G. and Szabo, A. (1982b) *J. Am. Chem. Soc.*, **104**, 4559–4570.

Liu, H., Tomas, P.D. and James, T.L. (1992) *J. Magn. Reson.*, **98**, 163–175.

Liu, H., Tonelli, M. and James, T.L. (1996) *J. Magn. Reson.*, **B111**, 85–89.

Macura, S. and Ernst, R.R. (1993) *Mol. Phys.*, **42**, 95–117.

Muhandiram, D.R. and Kay, L.E. (1993) *J. Magn. Reson.*, **B103**, 203–216.

Nerdal, W., Hare, D.R. and Reid, B.R. (1989) *Biochemistry*, **28**, 1008–1021.

Nikonowicz, E.P., Sirr, A., Legault, P., Jucker, F.M., Baer, L.M. and Pardi, A. (1992) *Nucleic Acids Res.*, **20**, 4515–4523.

Noggle, J.H. and Schirmer, R.E. (1971) *The Nuclear Overhauser Effect: Chemical Applications*, Academic Press, Inc., New York, NY.

Olejniczak, E.T. and Weiss, M.A. (1990) *J. Magn. Reson.*, **86**, 148–155.

Palmer, A.G., Cavanagh, J., Wright, P.E. and Rance, M. (1991) *J. Magn. Reson.*, **93**, 151–170.

Post, C.B., Meadows, R.P. and Gorenstein, D.G. (1990) *J. Am. Chem. Soc.*, **112**, 6796–6803.

Press, W.H., Flannery, B.P., Teukolsky, S.A. and Vetterling, W.T. (1989) *Numerical Recipes (FORTRAN version)*, Cambridge University Press, London/New York.

Schleucher, J., Schwendinger, M.G., Sattler, M., Schmidt, P., Schedletzky, O., Glaser, S.J., Sørensen, O.W. and Griesinger, C. (1994) *J. Biomol. NMR*, **4**, 301–306.

Stone, M.J., Chandrasekhar, K., Holmgren, A., Wright, P.E. and Dyson, H.J. (1993) *Biochemistry*, **32**, 426–435.

Tropp, J. (1980) *J. Chem. Phys.*, **72**, 6035–6043.

Wang, Y.-S. (1992) *Concepts Magn. Reson.*, **4**, 327–337.

Yip, P.F. and Case D.A. (1989) *J. Magn. Reson.*, **83**, 643–648.

Yip, P.F. and Case D.A. (1991) In *Computational Aspects of the Study of Biological Macromolecules by Nuclear Magnetic Resonance Spectroscopy* (Eds, Hoch, J.C., Poulsen, F.M. and Redfield, C.), Plenum Press, New York, NY.

Yip, P.F. (1993) *J. Biomol. NMR*, **3**, 361–365.

Zhu, L. and Reid, B.R. (1995) *J. Magn. Reson.*, **B106**, 227–235.

Zhu, L. (1996) *J. Magn. Reson.*, **B111**, 262–271.

Zimmer, D.P. and Crothers, D.M. (1995) *Proc. Natl. Acad. Sci. USA*, **92**, 3091–3095.

Zuiderweg, E.R. and Fesik, S.W. (1989) *Biochemistry*, **28**, 2387–2391.